scientific reports

Check for updates

OPEN

Comparative analysis of improved m6A sequencing based on antibody optimization for low-input samples

Jiafeng Lu[1,2], Wenjuan Xia[1,2], Jincheng Li[1], Liya Zhang[1], Chunfeng Qian[1], Hong Li[1]✉ & Boxian Huang[1]✉

The most effective method for mapping N6-methyladenosine (m^6A) is m^6A RNA immunoprecipitation sequencing (MeRIP-seq). The quality of MeRIP-seq relies on various factors, with the anti-m^6A antibody being a crucial determinant. However, comprehensive research on anti-m^6A antibody selection and optimal concentrations for different tissues has been limited. In this study, we optimized the concentration of five different anti-m^6A antibodies across various tissues. Our findings demonstrated that 5 µg of Millipore antibodies (ABE572 and MABE1006) performed well, starting from 15 µg total RNA from the liver, while 1.25 µg of Cell Signaling Technology antibodies (CST) (#56593) was suitable for low-input total RNA. In summary, we provide a significant guideline for anti-m^6A antibody selection in MeRIP sequencing for different tissues, especially in the context of low-input RNA.

Keywords m^6A antibody, MeRIP Seq, Human fetal brain, Human fetal liver, Mouse liver, Mouse brain

Abbreviations

MeRIP-seq	m^6A RNA immunoprecipitation sequencing
m^6A	N6-methyladenosine
miCLIP	m^6A individual-nucleotide-resolution cross-linking and immunoprecipitation
MAZTER-seq	RNA digestion via m^6A sensitive RNase
DART-seq	Deamination adjacent to RNA modification targets
3'UTR	Three prime untranslated region
GTEx	Genotype-Tissue Expression
TiGER	Tissue-specific Gene Expression Regulation

RNAs undergo more than 150 distinct posttranscriptional modifications, with N6-methyladenosine (m^6A) methylation being the most prevalent internal chemical modification in messenger RNA (mRNA)[1,2]. Playing a pivotal role in various biological processes like cell differentiation, embryogenesis, and disease[3–5], m^6A modification is a reversible and dynamic process catalyzed by the m^6A methyltransferase complex, comprising METTL3 and METTL14[6]. Remarkably, a reduction in METTL3 has been linked to inhibited spermatogenesis and oocyte maturation[7,8], while METTL14 is essential for mammalian embryogenesis[9].

Conversely, m^6A demethylation is carried out by m^6A demethylases, including FTO and ALKBH5. The m^6A demethylation mediated by the fat mass and obesity associated (FTO) gene affects the expression of transcription factors, influencing autophagy regulation in tumors[10]. Additionally, m^6A can be recognized by m^6A binding proteins, specifically proteins of the YTH domain family (YTHDC1/2 and YTHDF1/2/3). These YTH domain proteins play a role in mRNA translation and promote cell proliferation by binding to m^6A-modified mRNA[11,12].

The most widely used transcriptome-wide m^6A profiling method, MeRIP-seq, has been applied in various cell lines and tissues across multiple species[13,14]. In this RNA immunoprecipitation assay, RNA fragmentation is followed by immunoprecipitation of m^6A-modified RNA fragments. After extensive high/low salt washing, the eluted RNA fragments are used to construct an m^6A library. However, MeRIP-seq has some limitations, for example, sequencing RNA fragments typically allows mapping the orientation of m^6A at a resolution of 100–200 nt. To enhance the accuracy of m^6A position mapping, miCLIP, based on cross-linking and immunoprecipitation, was developed for single-nucleotide detection[15]. While miCLIP offers superior m^6A resolution compared to MeRIP-seq, it entails a labor-intensive process and requires a substantial amount of starting material. Recently, novel antibody-independent m6A identification strategies, such as MAZTER-seq[16] and DART-seq[17], have been

[1]State Key Laboratory of Reproductive Medicine, Suzhou Municipal Hospital, Suzhou Affiliated Hospital of Nanjing Medical University, Gusu School, Nanjing Medical University, Suzhou 215002, China. [2]Jiafeng Lu and Wenjuan Xia contributed equally to this work. ✉email: ; huangboxiannj@163.com; hongliszivf@163.com

introduced for global m^{6}A profiling. MAZTER-seq utilizes MazF RNase to cleave RNA at unmethylated sites containing ACA motifs, leaving the unmethylated sites unchanged. Although allowing quantitative tracking of m^{6}A at single-nucleotide resolution, MAZTER-seq only detects 16-25% of all m^{6}A methylation sites[16]. DART-seq enables m^{6}A detection through APOBEC1-YTH binding and C-to-U editing, but the expression and purification of the APOBEC1-YTH protein pose challenges[17]. Nevertheless, MeRIP-seq remains more popular than other m^{6}A detection methods due to its relatively simple protocol and wide applicability for low-input starting materials, as low as 2 μg of total RNA, through optimization of different parameters[18].

Currently, conventional MeRIP-seq typically necessitates 300 μg of total RNA for subsequent intricate processes, leading to significant RNA loss. Despite reducing the starting total RNA to 2 μg by optimizing key parameters[18], the best-performing m^{6}A antibody (Millipore, ABE572) has unfortunately been discontinued. Monoclonal or polyclonal m^{6}A antibodies serve as the master reagent in MeRIP-seq. Generally, polyclonal antibodies comprise a mixed group with varied activities and exhibit superior affinity, while monoclonal antibodies recognize a defined epitope with specific specificity and affinity[19–21]. Given that m^{6}A is a relatively small molecule with minimal immunogenicity, accurately identifying and capturing it poses a challenge for m^{6}A antibodies. To address these limitations, our study aims to enhance MeRIP-seq performance by systematically evaluating and optimizing the concentration of commercially available m^{6}A antibodies. Specifically, we seek to provide practical guidelines for selecting appropriate antibody concentrations to maximize m^{6}A enrichment accuracy, particularly for low-input RNA samples from diverse organs and species. These efforts aim to ensure reliable and reproducible m6A profiling for epitranscriptomic studies, even under suboptimal conditions.

Results

M572 demonstrated superior performance with standard amounts of liver RNA, while CST exhibited significant potential with low amounts of mouse brain RNA.

Since anti-m^{6}A antibodies play a crucial role in the capture efficiency of m^{6}A-containing RNA fragments, we selected five commonly used anti-m^{6}A antibodies for a comprehensive performance comparison. To assess their effectiveness across different tissues and species, we focused on two representative organs, the liver and brain, from human fetuses and mice in the subsequent optimized MeRIP-seq (Fig. 1A). The optimized MeRIP-seq involved extensive high/low salt washing after incubation of the antibody-bead complex and RNA fragments. Subsequently, the SMARTer Stranded Total RNA-Seq Kit v2 (Pico Input Mammalian) was used for library construction, following a previously reported protocol[18] (Fig. 1A). Initially, we successfully constructed thirty-five MeRIP-seq libraries, comprising twenty-nine RIP and six corresponding input RNA samples, using five anti-m^{6}A antibodies (Darmstadt, Germany, Millipore, ABE572, Darmstadt, Germany, Millipore, MABE1006, Goettingen, Germany, Synaptic Systems, 202003, Danvers, Massachusetts, USA, Cell Signaling Technology, #56593, Waltham, Massachusetts, USA, Thermo Fisher Scientific, MA5-33030). These anti-m^{6}A antibodies are abbreviated as M572, M1006, SY, CST, and THER, respectively (Fig. 1A). Subsequently, we analyzed and compared the number of m^{6}A peaks and m^{6}A-modified genes using 15 μg total RNA from human fetal liver among the five antibodies (the regular amount of anti-m^{6}A antibody was 5 μg). Interestingly, the five antibodies exhibited distinct numbers of m^{6}A peaks and genes, with M572 identifying the most m^{6}A peaks and genes in human fetal liver. In contrast, M1006 detected fewer m^{6}A peaks and genes than M572, and SY, CST, and THER showed significant reductions in both aspects (Fig. 1B). A similar trend was observed in adult mouse livers (Fig. 1C). However, in the adult mouse brain, CST obtained more m^{6}A peaks compared to M572 (Fig. 1D). Clearly, the efficiency of capturing m^{6}A-containing RNA fragments varies among antibodies derived from different tissues (Fig. 1B-D). Additionally, we calculated the modified level of the m^{6}A genes for each antibody in the adult mouse brain and found that CST had more unique m^{6}A genes, while M572, CST, M1006, and SY shared quite a few overlapping common m^{6}A genes (Figure S1A). Furthermore, we mapped the m^{6}A genes of the five antibodies onto human and mouse chromosomes. Additionally, we plotted the m^{6}A genes associated with the five antibodies on human and mouse chromosomes. While the distribution of m^{6}A genes on each chromosome followed a pattern similar to that observed in Fig. 1B and D (Figure S1H-J), the distribution of m^{6}A genes was consistent across chromosomes (Figure S1E-G). Notably, M572 exhibited a high percentage of captured m^{6}A genes on chromosome twelve in the adult mouse liver (Figure S1I).

Subsequently, we observed that enriched m^{6}A peaks exhibited a preference for clustering near the stop codon, and this distribution pattern of m^{6}A peaks was consistent among the five antibodies in different tissues (Figure S1B-D), aligning with previous studies[22]. These findings suggested that we obtained highly reliable m^{6}A genes with the exception of THER among the five antibodies. We then investigated the distribution of differential m^{6}A peaks in the genome and observed that a higher percentage of m^{6}A peaks from M572 tended to be enriched in the 3'UTRs compared to other antibodies in the human fetal liver (Fig. 1E). Furthermore, the proportion of m^{6}A peaks enriched in the 3'UTRs notably increased for M572 compared to the other antibodies, particularly in the adult mouse liver and brain (Fig. 1F, G). Concurrently, M1006, SY, and CST exhibited similar m^{6}A peak enrichment in the 3'UTRs and exons across different tissues (Fig. 1E-G).

In summary, M572 demonstrated notable advantages in regular amounts of RNA from human fetal and mouse liver. However, for routine MeRIP sequencing, M1006 or CST could serve as suitable alternatives. CST also exhibited promising potential in low amounts of RNA from the mouse brain, with comparable performance to M572 or M1006. CST's potential in low-input RNA scenarios is particularly noteworthy given the challenges in m^{6}A profiling when sample availability is limited. Many experimental designs, especially those involving rare tissues, single cells, or small-scale samples, face constraints in RNA quantity, which often hampers data reliability and reproducibility. CST's ability to achieve significant m^{6}A enrichment under such conditions highlights its utility for applications where RNA input is a limiting factor. CST's strong performance at low RNA concentrations makes it a promising candidate for single-cell or single-nucleus m^{6}A sequencing studies. This

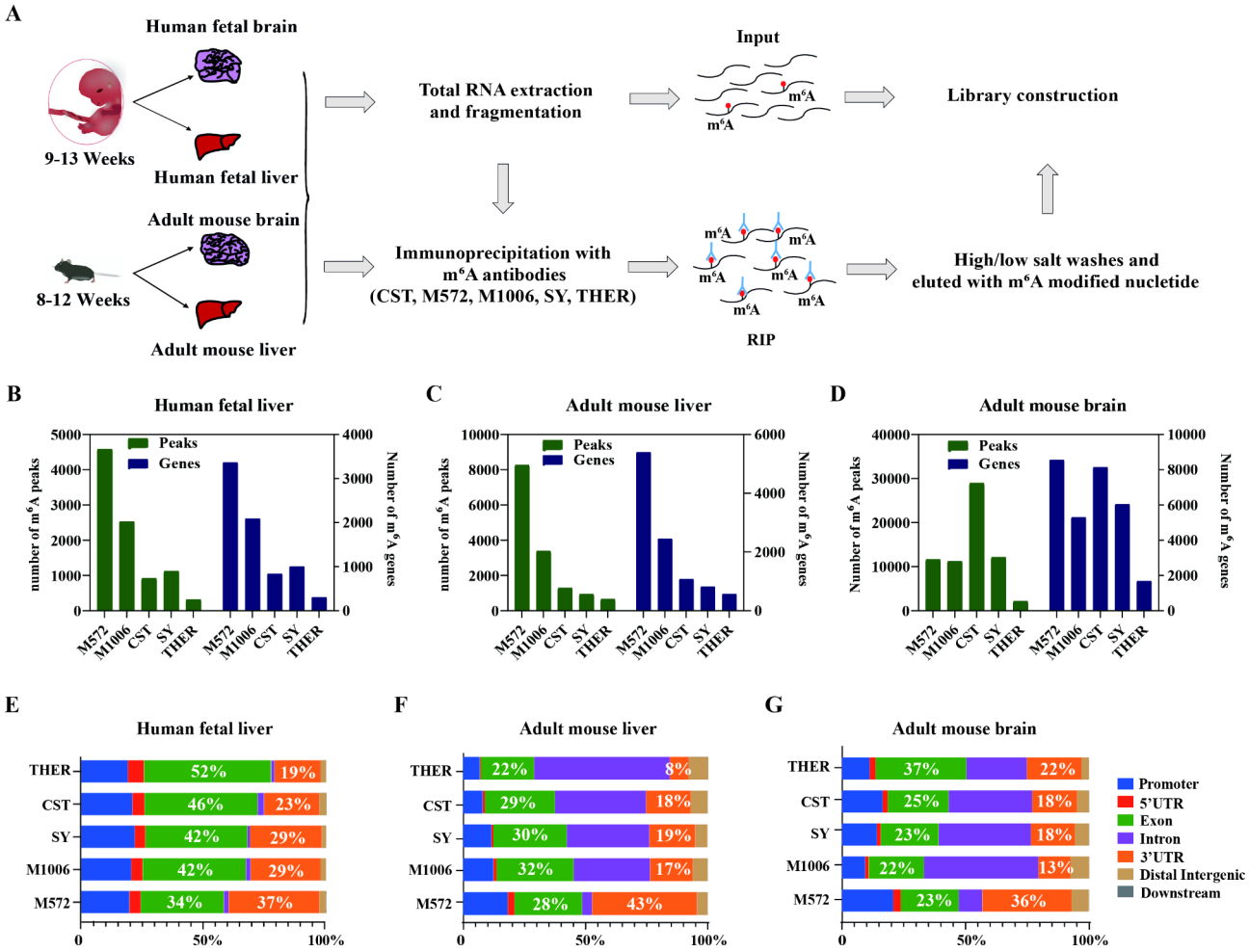

Fig. 1. Overall differential m^{6}A profiling in human fetal and mouse livers with five anti-m^{6}A antibodies. (**A**) Schematics of the selected organs, such as the livers and brains of human fetuses (9–13 gestational weeks) and mouse (8–12 weeks after birth), and the procedure of improved MeRIP sequencing for low-input samples. (**B**) The total number of m^{6}A peaks and m^{6}A genes of libraries constructed from five antibodies in human fetal liver. (**C**) The total number of m^{6}A peaks and m^{6}A genes in libraries constructed from five antibodies in the livers of adult mice. (**D**) The total number of m^{6}A peaks and m^{6}A genes in libraries constructed from five antibodies in the brains of adult mice. (**E**) The percentage of m^{6}A peaks belonging to five libraries in human fetal liver distributed across different genomic regions, including the promoter, 5' UTR, exon, intron, 3' UTR, distal intergenic and downstream regions. (**F**) The percentage of m^{6}A peaks belonging to five libraries in the livers of adult mice distributed across different genomic regions. (**G**) The percentage of m^{6}A peaks belonging to five libraries in the brains of adult mice distributed across different genomic regions.

application could provide high-resolution insights into cell-type-specific m^{6}A patterns in complex tissues such as the brain.

M572, M1006, and CST: high enrichment of m6A levels and tissue-specific m6A genes

Next, we analyzed the pattern of enriched m^{6}A methylation among the five antibodies. Notably, both M572 and M1006 exhibited significantly higher m^{6}A enrichment peaks, ranking as the top two antibodies in both human fetal liver and mouse liver (Fig. 2A and B). In contrast, the other three antibodies displayed comparatively lower m^{6}A enrichment levels (Fig. 2A and B). Interestingly, M572 and CST demonstrated superior abilities to enrich m^{6}A peaks in the adult mouse brain compared to the other antibodies (Fig. 2C), aligning with the earlier findings (Fig. 1D). Additionally, we calculated the counts of unique and overlapping tissue-specific m^{6}A genes based on Genotype-Tissue Expression (GTEx) and Tissue-specific Gene Expression Regulation (TiGER). Notably, M572 exhibited the highest counts of overlapping liver-specific m^{6}A genes (approximately 120), surpassing M1006, SY, CST, and THER (Fig. 2D). This trend continued in the adult mouse liver, where M572 also showed the highest counts of overlapping and unique liver-specific m^{6}A genes among the five antibodies (Fig. 2E). Furthermore, in the adult mouse brain, M572, M1006, CST, and SY displayed similar numbers of unique m^{6}A genes, as well as overlapping brain-specific m^{6}A genes, whereas THER exhibited a lower count (Fig. 2F).

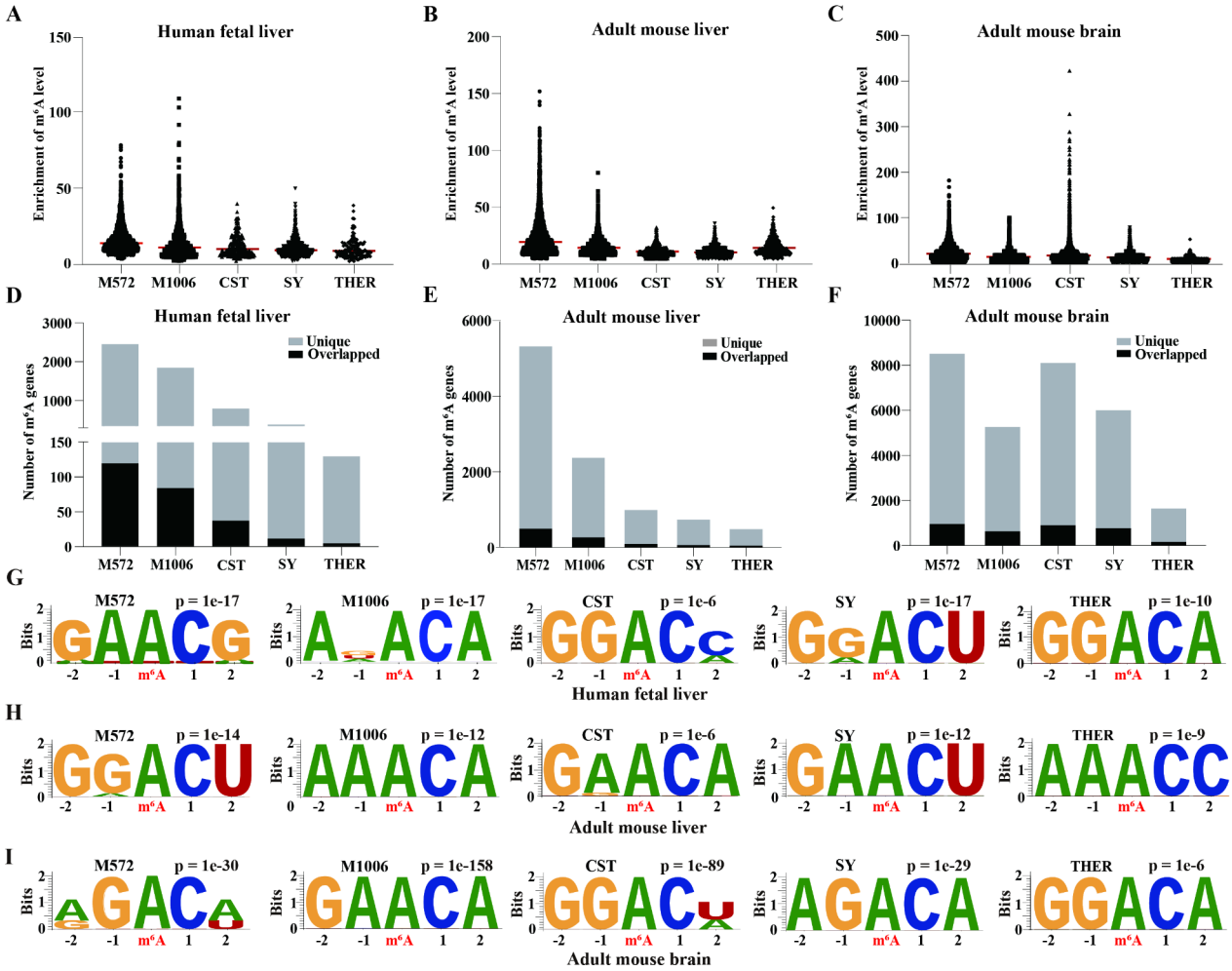

Fig. 2. Distribution of enriched m^{6}A level and m^{6}A motifs as well as tissue-specific m^{6}A genes among five anti-m^{6}A antibodies. (**A**) The distribution of enriched m^{6}A level among five antibodies in human fetal liver. (**B**) The distribution of enriched m^{6}A level among five antibodies in adult mouse liver. (**C**) The distribution of enriched m^{6}A level among five antibodies in the adult mouse brain. (**D**) The overlapped and unique human liver-specific m^{6}A genes obtained with five antibodies in human fetal liver. (**E**) The overlapping and unique mouse liver-specific m^{6}A genes obtained with five antibodies in adult mouse livers. (**F**) The overlapped and unique mouse brain-specific m^{6}A genes obtained with five antibodies in the adult mouse brain. (**G**) Sequence motifs identified within m^{6}A peaks across five antibodies in human fetal liver. (M572, p value = 1e^{-17}, M1006, p value = 1e^{-17}, CST, p value = 1e^{-6}, SY, p value = 1e$^{-17,}$ THER, p value = 1e^{-10}). H, Sequence motifs identified within m^{6}A peaks across five antibodies in adult mouse liver. (M572, p value = 1e^{-14}, M1006, p value = 1e^{-12}, CST, p value = 1e^{-6}, SY, p value = 1e$^{-12,}$ THER p value = 1e^{-9}). I, Sequence motifs identified within m^{6}A peaks across five antibodies in the adult mouse brain. (M572, p value = 1e^{-30}, M1006, p value = 1e^{-158}, CST, p value = 1e^{-89}, SY, p value = 1e$^{-29,}$ THER, p value = 1e^{-6}). Key findings: M572 and M1006 consistently show superior performance in terms of enriched m^{6}A levels and the identification of tissue-specific m^{6}A genes across human and mouse liver tissues. CST excels in the adult mouse brain, highlighting the importance of selecting the appropriate antibody depending on the tissue type. The identification of distinct consensus motifs across tissues underscores the tissue-specific nature of m^{6}A modifications and the variability in antibody performance. Implications: Fig. 2 provides a comprehensive overview of antibody performance in detecting m^{6}A modifications across tissues, emphasizing their tissue-specific strengths and revealing critical insights into the biology of m^{6}A.

Early studies have indicated that m^{6}A transcripts commonly exhibit a conserved "RRACH" motif (R = G/A, H = A/U/C). Therefore, we examined the most likely consensus motif for m^{6}A among the five antibodies in three tissues. Notably, we observed distinct distribution patterns for the most likely consensus motif for m^{6}A among the antibodies. For example, in human fetal liver, "GGACH" emerged as the most frequent consensus motif (Fig. 2G), while in mouse liver, "RAACH" dominated the consensus motif landscape (Fig. 2H). Among the "RRACH" m^{6}A consensus motifs, "GGACH" stands out as the most frequent and core motif in tissues[13]. These findings suggest that the m^{6}A consensus motifs of different anti-m^{6}A antibodies are conserved in human tissues, such as the fetal liver, but divergent in mouse tissues, including the liver and brain. When considering

the consensus motif and related *p*-value, M572, M1006, and SY consistently ranked in the top three, not only in human fetal liver but also in adult mouse liver (Fig. 2G and H). However, in the adult mouse brain, M1006, CST, and M572 emerged as the superior antibodies (Fig. 2I). It is worth noting that, despite M572 having a relatively low *p*-value, its consensus motifs in the three organs displayed diversity (Fig. 2G, H and I).

In summary, M572 and M1006 exhibited higher enrichment of m^{6}A levels and tissue-specific m^{6}A genes, along with consensus motifs, compared to the other three antibodies in the liver. As mentioned earlier, CST displayed favorable performance in the mouse brain. Using CST at lower concentrations allows for the reduction of antibody and material costs while still obtaining high-quality data. This could be particularly advantageous in large-scale experiments, such as in high-throughput screening or studies involving small sample sizes. Moreover, CST's versatility could make it an ideal choice for large-scale, multi-tissue studies, where optimizing RNA input is crucial to maximize efficiency and reduce costs.

M572 and M1006 excelled in the liver, while CST performed similarly to M572 in the mouse brain

Since m^{6}A peaks were not evenly distributed on a transcriptome-wide scale, we further examined the adenosine methylation pattern within transcripts. The majority of m^{6}A genes displayed a single m^{6}A peak (Fig. 3A, D and G). In the group with one m^{6}A peak, M572 and M1006 exhibited similar gene numbers (Fig. 3A). For the group with two m^{6}A peaks, M572 had the highest number, followed by SY, with the other three antibodies showing similar counts (Fig. 3A). In groups with three or more m^{6}A peaks, M572 dominated, while the counts for the other three antibodies were significantly lower (Fig. 3A). In mouse liver, M572 outperformed in all four groups with different m^{6}A peak numbers (Fig. 3D). M1006 had a notably lower count than M572 in the single peak group and showed a sparse pattern in the other three groups (Fig. 3D). In the mouse brain, while M572, M1006, CST, and SY had similar m^{6}A gene numbers in groups with a single or two peaks, CST surpassed in the group with four or more peaks (Fig. 3E). Next, we investigated the pattern of highly methylated m^{6}A transcripts. In both human fetal liver and mouse liver, the number of enriched m^{6}A genes (score > 10 and score > 20) was consistently highest for M572, followed by M1006, CST, SY, and THER (Fig. 3B and E). In the mouse brain, the number of enriched m^{6}A genes in CST significantly increased, ranking second only to M572 (Fig. 3H). To illustrate the similarity and heterogeneity of m^{6}A genes, a Venn diagram was created. The overlap of m^{6}A genes was low (35 genes) between the five antibodies in human fetal liver (Fig. 3C), but relatively higher (208 genes) in the mouse liver (Fig. 3F). Moreover, the number of unique m^{6}A genes (2892) in CST significantly exceeded those of the other four antibodies in the adult mouse brain (Fig. 3I). These findings indicate that M572 still holds superiority in both enriched m^{6}A peaks and m^{6}A genes within transcripts, while M1006 closely follows in the liver. In the mouse brain, CST's performance is comparable to that of M572 and M1006.

A relatively low concentration of CST performed well in the human fetal brain starting from low-input materials

While M572 demonstrated superior performance in most of the aforementioned analyses, the complexity of the polyclonal antibody composition may lead to diverse results. Consequently, based on the earlier discussions, we opted for M1006 and CST as two monoclonal antibodies to conduct further optimized experiments with low-input total RNA (15 μg) from the human fetal brain. Initially, we selected different concentrations of CST (1.25 μg, 2.5 μg, and 5 μg) and M1006 antibody (2.5 μg and 5 μg) to conduct MeRIP-seq with 15 μg of total RNA from the human fetal brain. The results showed that the number of m^{6}A peaks and m^{6}A genes in the 5 μg M1006 group was significantly higher than those in the 2.5 μg M1006 group (Fig. 4A). To the contrary, the number of m^{6}A peaks and genes in the 1.25 μg CST library was much higher than those in the 2.5 μg and 5 μg CST libraries, and it was comparable to the 5 μg M1006 group (Fig. 4A). To confirm if a similar phenomenon exists in the mouse brain, we measured the m^{6}A level via m^{6}A dot blot in mouse brains treated with M1006 and CST at different concentrations (Fig. 4B). As anticipated, when the initial amount of total RNA was reduced, the expression of m^{6}A decreased for M1006 at a fixed concentration of 5 μg/mL (Fig. 4A). Surprisingly, CST exhibited an unexpected characteristic, with the detected m^{6}A level increasing as the concentration of CST was reduced from 5 μg/mL to 1 μg/mL (Fig. 4B), regardless of the starting RNA amount (5 μg, 2 μg, 1 μg, or 500 ng). A similar phenomenon was also observed in the mRNA from mouse brain tissue using dot blot analysis (Figure S2). Based on these observations, we hypothesized that a regular concentration of M1006 (5 μg) and a reduced concentration of CST (1.25–2.5 μg) might perform well in the brain with 15 μg of total RNA. Notably, the m^{6}A enrichment peaks of 5 μg M1006 ranked highest among the five groups (Fig. 4C). Additionally, the number of enriched m^{6}A peaks increased as the concentration of CST antibody was reduced from 5 μg to 1.25 μg (Fig. 4C). Moreover, the percentage of m^{6}A peaks enriched in the 3'UTR of CST decreased gradually as the concentration of CST changed from 1.25 μg to 5 μg, while the trend of M1006 was inversely proportional to its concentration (Fig. 4D). To confirm the effectiveness of obtaining m^{6}A peaks, we selected three neuro-related genes, *Sox2*, *Snurf* and *Map2*, for IGV screenshots of m^{6}A peaks. We found that M1006-5 μg antibody library exhibited distinct enrichment of m^{6}A peaks specifically on *Sox2*. Notably, the CST-1.25 μg library displayed significant enrichment of m^{6}A peaks on *Snurf*. Shared m^{6}A peaks were identified in the *Map2* region between the M1006-5 μg and CST-1.25 μg libraries (Fig. 4E). In the four groups of m^{6}A genes with different peaks, the number of m^{6}A genes with 5 μg M1006 was consistently the highest among the five antibodies (Fig. 4F). Notably, in the group of one m^{6}A peak, the number of m^{6}A genes in 1.25 μg CST was much higher than in 2.5 μg CST, while in the other three groups of m^{6}A peaks, the number of m^{6}A genes in both concentrations was similar (Fig. 4F). As anticipated, the m^{6}A peaks preferentially appeared around stop codons in all groups (Fig. 4G). Furthermore, to investigate the overlapping m^{6}A genes between the five groups, we generated an UpSet plot using the R package, revealing considerable overlaps of shared m^{6}A genes between the two antibodies at different concentrations (Fig. 4H).

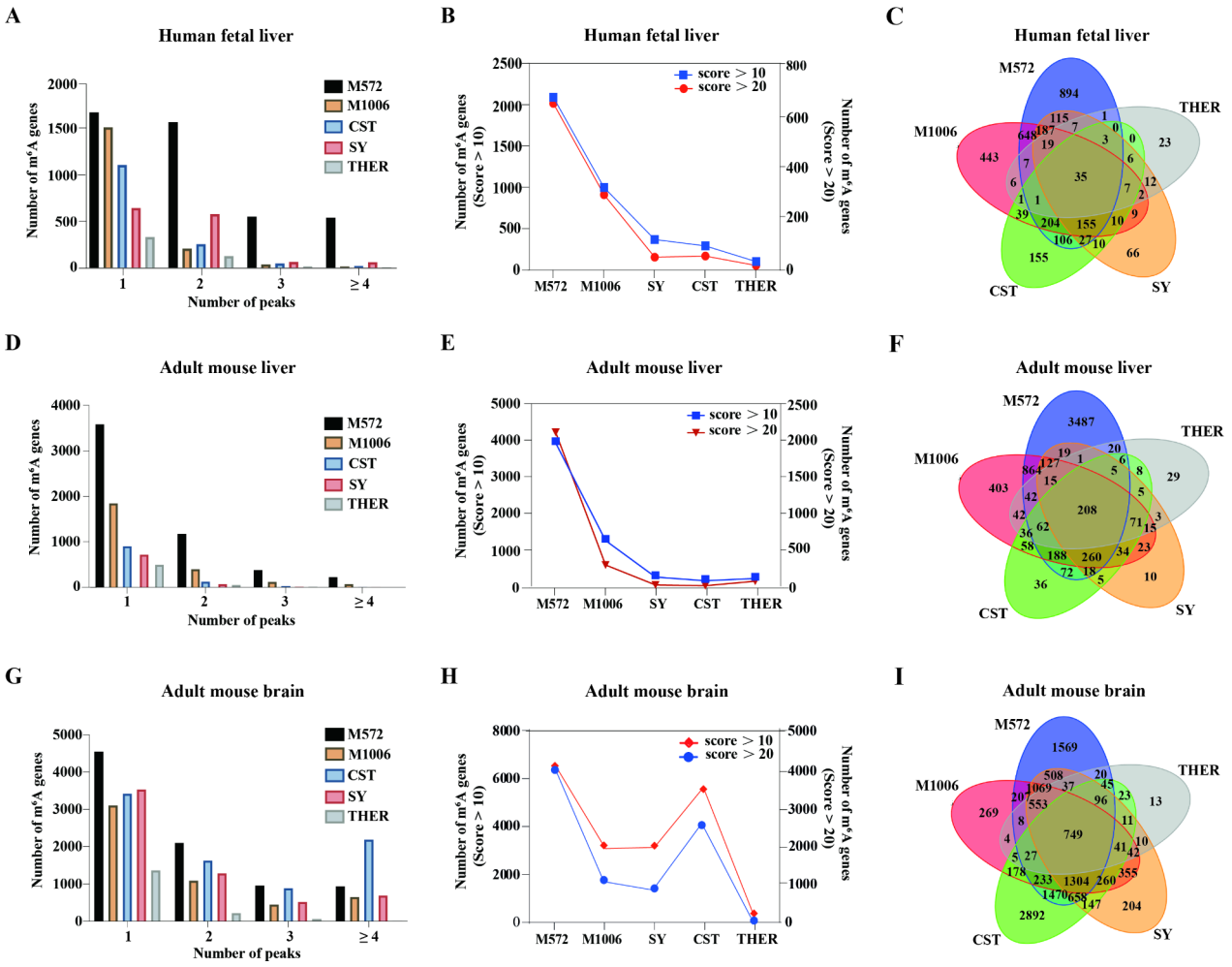

Fig. 3. Diverse numbers of m^{6}A peaks within transcripts and m^{6}A genes of high expression (gene score > 10 and gene score > 20). (**A**) Histogram of m^{6}A genes that contain one or more m^{6}A peaks (peak = 1, peak = 2, peak = 3, and peak ≥ 4) in human fetal liver. (**B**) The counts of m^{6}A genes (score > 10 and score > 20) among five antibodies in human fetal liver. (**C**) Venn diagram showing the overlap of m^{6}A-containing genes across five antibodies in human fetal liver. (**D**) Histogram of m^{6}A genes that contain one or more m^{6}A peaks (peak = 1, peak = 2, peak = 3, and peak ≥ 4) in mouse liver. (**E**) The counts of m^{6}A genes (score > 10 and score > 20) among five antibodies in mouse liver. (**F**) Venn diagram showing the overlap of m^{6}A-containing genes across five antibodies in mouse liver. (**G**) Histogram of m^{6}A genes that contain one or more m^{6}A peaks (peak = 1, peak = 2, peak = 3, and peak ≥ 4) in the mouse brain. (**H**) The counts of m^{6}A genes (score > 10 and score > 20) among five antibodies in the mouse brain. (**I**) Venn diagram showing the overlap of m^{6}A-containing genes across five antibodies in the mouse brain. These findings highlight the exceptional performance of M572 in detecting both enriched m^{6}A peaks and highly expressed m^{6}A-containing genes, particularly in human fetal liver and mouse liver, demonstrating its utility for epitranscriptomic studies in liver tissues.

In summary, both M1006 at a regular concentration of 5 μg and CST at a relatively low concentration of 1.25 μg exhibited better performance in various aspects in the human fetal brain.

CST at lower concentrations excels in low-input MeRIP libraries from human fetal liver

The reduced concentration of CST unexpectedly exhibited excellent performance in the human fetal brain with low-input materials. To validate that this notable performance was not a coincidence, we specifically selected the CST antibody and optimized its concentrations for constructing a library from low-input RNA in the human fetal liver. Initially, we selected different concentrations of CST (1.25 μg, 2.5 μg, and 5 μg) and conducted MeRIP-seq with 15 μg of total RNA from the human fetal liver. In line with the brain results, the number of m^{6}A peaks and genes in the 1.25 μg CST library were slightly higher than those in the 2.5 μg CST library and significantly higher than those in the 5 μg CST library (Fig. 5A). Subsequently, we assessed the m^{6}A levels using a dot blot in mouse livers treated with different concentrations of CST and M1006 (Fig. 5B). Notably, M1006 proved unsuitable for low-input RNA from mouse liver (Fig. 5B). Excitingly, the m^{6}A level remained remarkably consistent at a CST concentration of 1 μg/mL, irrespective of the initial RNA quantity (5 μg, 2 μg, 1 μg, and 500 ng). (Fig. 5B), consistent with the results observed in the mouse brain (Fig. 4B). Using GTEx and TiGER,

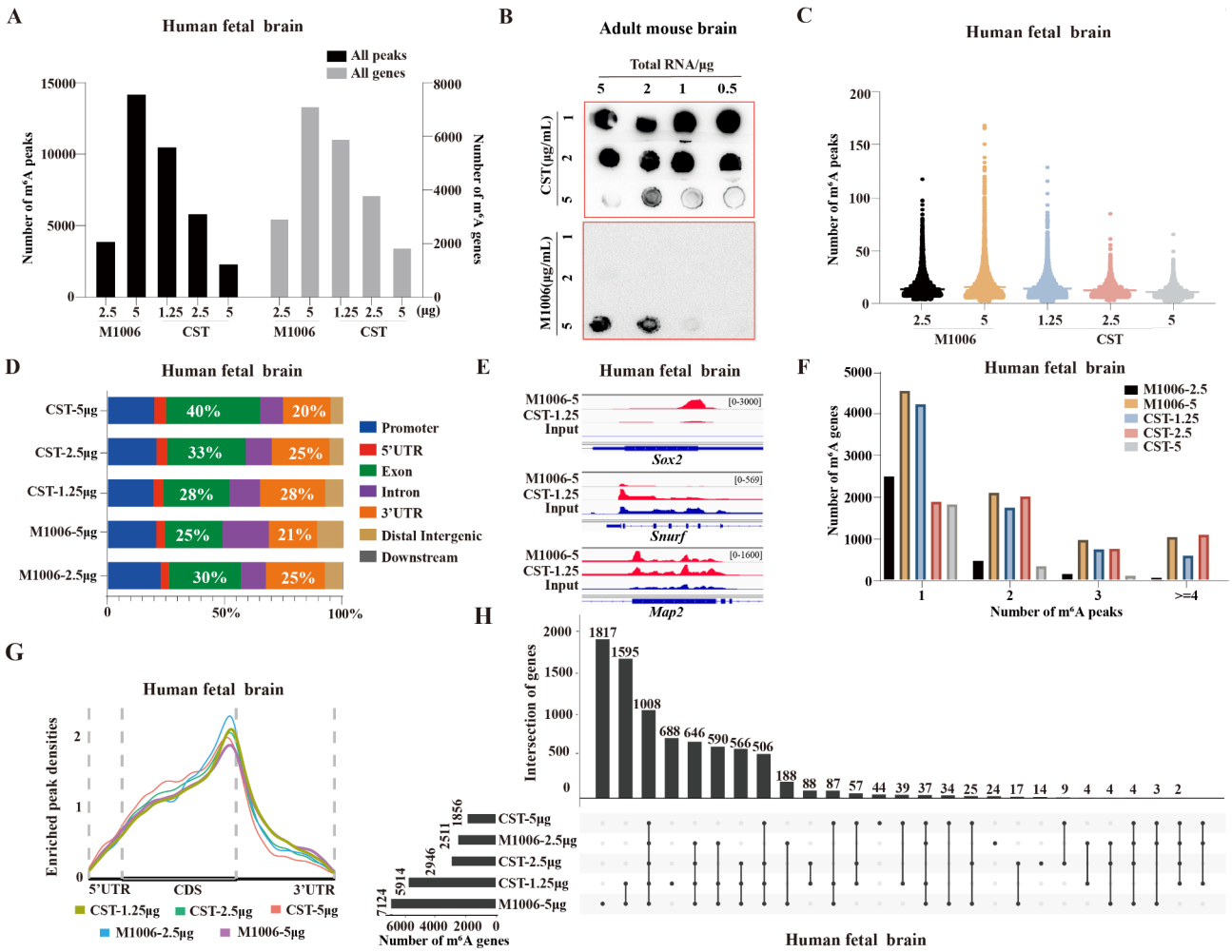

Fig. 4. Optimization of CST and M1006 antibody to construct MeRIP-seq libraries from human fetal brain. (**A**) The counts of the m^{6}A peak and m^{6}A gene were expressed in the M1006 (2.5 μg and 5 μg) and CST (1.25 μg, 2.5 μg and 5 μg) libraries from the human fetal brain. (**B**) The m^{6}A level of total RNA from the mouse brain was indicated by m^{6}A dot blot. Corresponding total RNAs were loaded equally by a serial dilution with 5 μg, 2 μg, 1 μg and 500 ng; the corresponding antibodies were CST and M1006 (concentration at 1 μg/mL, 2 μg/mL, 5 μg/mL). (**C**) The distribution of enriched m^{6}A level of two antibodies at different concentrations. (**D**) The distribution of m^{6}A peaks in the human fetal brain was analyzed, considering different genomic regions, such as the promoter, 5' UTR, exon, intron, 3' UTR, distal intergenic, and downstream regions, for two antibodies at varying concentrations. (**E**) IGV screenshots illustrating the m^{6}A peaks of *Sox2*, *Snurf*, and *Map2* for M1006-5 μg and CST-1.25 μg. (**F**) Histogram of m^{6}A genes that contain one or more m^{6}A peaks (peak = 1, peak = 2, peak = 3, and peak ≥ 4) of two antibodies at different concentrations in the human fetal brain. (**G**) Distribution of the enriched m^{6}A peaks of two antibodies at different concentrations in the human fetal brain. (**H**) UpSet diagram showing the overlapping m^{6}A genes in two antibodies at different concentrations in the human fetal brain. These findings highlight the exceptional performance of M572 in detecting both enriched m^{6}A peaks and highly expressed m^{6}A-containing genes, particularly in human fetal liver and mouse liver, demonstrating its utility for epitranscriptomic studies in liver tissues.

we observed that the count of m^{6}A genes in the 1.25 μg CST library consistently surpassed the counts of the other two higher CST concentrations, encompassing unique m^{6}A genes and overlapping liver-specific m6A genes (Fig. 5C). Furthermore, the percentage of m^{6}A peaks enriched in the 3'UTR increased from 23 to 32% with the reduction of CST concentration from 5 μg to 1.25 μg (Fig. 5D). The characteristic m^{6}A distribution patterns, with enrichment near the stop codons, were consistently observed for CST at different concentrations (Fig. 5E). Additionally, the number of m^{6}A genes distributed across every chromosome at 1.25 μg CST was markedly higher than at 2.5 μg and 5 μg CST (Fig. 5F). The modified level of the m^{6}A genes for CST at different concentrations were then analyzed, revealing that 1.25 μg CST not only encompassed the majority of the m^{6}A gene at 2.5 μg and 5 μg but also contained numerous unique m^{6}A gene (Fig. 5G).

In summary, a reduced concentration of CST (1.25 μg) outperformed higher concentrations in terms of enriched m^{6}A peaks and m^{6}A genes in the human fetal liver.

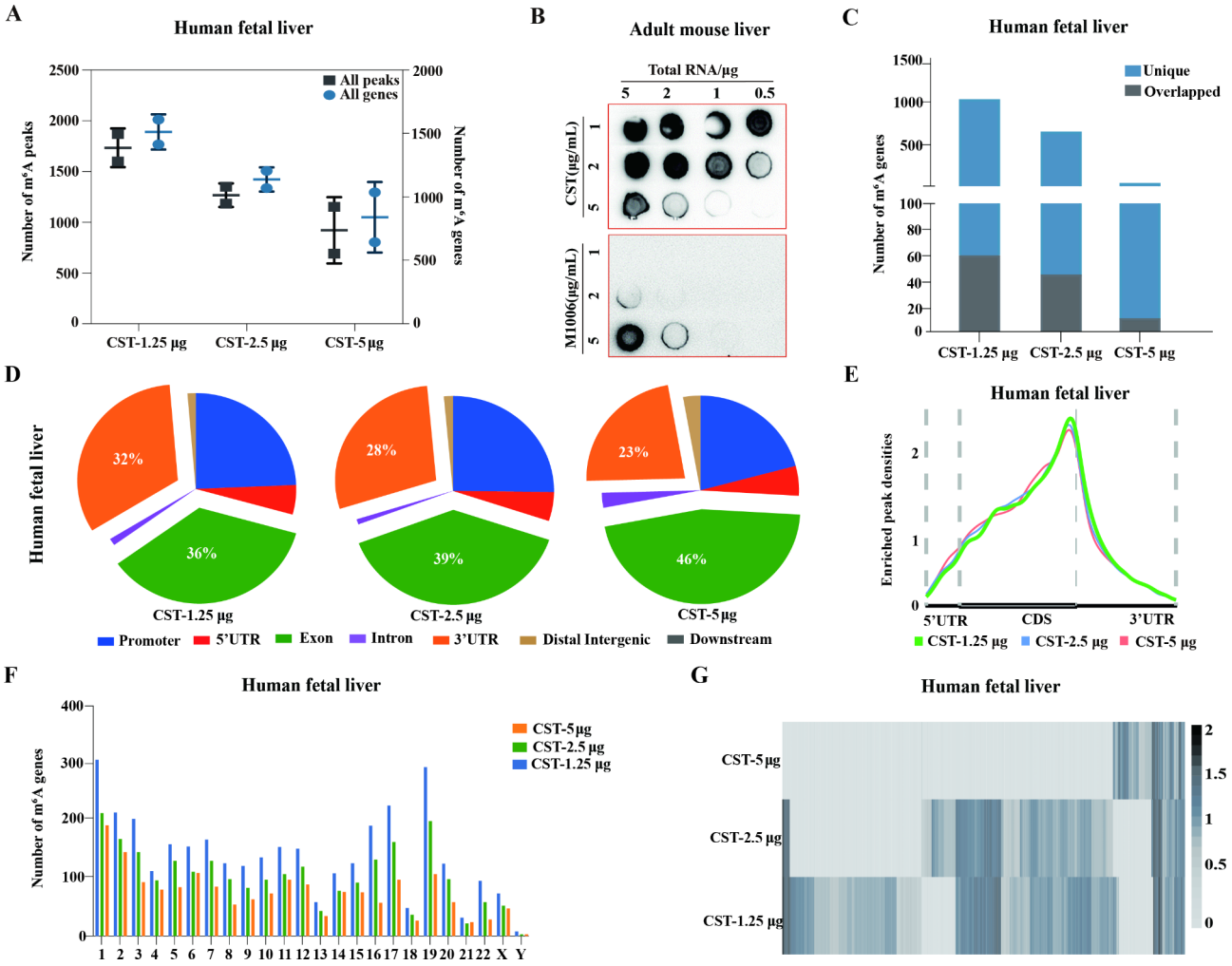

Fig. 5. Concentration optimization of CST to construct low-input MeRIP-seq from human fetal liver. (**A**) The counts of m^{6}A peaks and m^{6}A genes were measured in the CST (1.25 μg, 2.5 μg, and 5 μg) libraries derived from the human fetal liver. (**B**) The m^{6}A level of total RNA from mouse liver was indicated by m^{6}A dot blot. Corresponding total RNA was loaded equally by serial dilutions of 5 μg, 2 μg, 1 μg and 500 ng; the corresponding antibodies were CST and M1006 antibody (concentrations of 1 μg/mL, 2 μg/mL, and 5 μg/mL). (**C**) The overlapped and unique human liver-specific m^{6}A genes obtained with CST (1.25 μg, 2.5 μg and 5 μg) in human fetal liver. (**D**) The percentage of m^{6}A peaks belonging to CST (1.25 μg, 2.5 μg and 5 μg) in human fetal liver distributed across different genomic regions, including the promoter, 5' UTR, exon, intron, 3' UTR, distal intergenic and downstream regions. (**E**) Distribution of the enriched m^{6}A peaks of CST (1.25 μg, 2.5 μg and 5 μg) in the human fetal liver. (**F**) Distribution of m^{6}A genes of CST (1.25 μg, 2.5 μg and 5 μg) on chromosomes. (**G**) Heatmap of of the m^{6}A scores of CST (1.25 μg, 2.5 μg and 5 μg).

Discussion

In this study, we conducted a comprehensive comparison of the performance of five commercial anti-m^{6}A antibodies in the liver and brain from human fetuses and adult mice, considering different concentrations. Our findings reaffirmed the superior performance of the discontinued M572 antibody, consistent with previous reports[18]. Given the unavailability of M572 and the need for low-input starting RNA from limited clinical samples, we optimized the concentrations of CST and M1006, two monoclonal antibodies, for MeRIP-seq using 15 μg total RNA from both human fetal brain and liver. While a regular concentration of M1006 yielded satisfactory results for the human fetal brain in MeRIP-seq, the dot blot results for m^{6}A levels with M1006 were notably less favorable than those obtained with CST at reduced concentrations in the mouse brain and liver. Intriguingly, the CST antibody, particularly at a low concentration (1.25 μg), exhibited excellent performance in terms of m^{6}A levels and MeRIP-seq starting from low-input total RNA (15 μg) in both the human fetal brain and liver.

Recent advancements in research have enabled large-scale, transcriptome-wide identification of m^{6}A. For anti-m^{6}A antibodies to serve as reliable tools, they need thorough validation for their intended use, considering variations in tissues or species. A systematic comparison between anti-m^{6}A polyclonal and monoclonal antibodies has been lacking until now. Studies on antibodies targeting posttranslational histone modifications

have indicated that monoclonal antibodies offer similar sensitivity but higher reproducibility compared to polyclonal antibodies[23]. Polyclonal antibodies generally perform well with high initial total RNA due to their adaptability under complex conditions. They often exhibit an extensive but less well-characterized pattern of interaction. In contrast, monoclonal antibodies typically recognize a defined epitope with specific and known affinity. While RNA nucleotides are too small to induce immune responses, constructing antibodies targeting single nucleosides is possible by coupling proteins with immunogenic carriers. The carrier protein used for coupling may influence the antibody titer of anti-m^{6}A antibodies. Antibody titer is a measure of the inverse of the greatest dilution level for a positive result[24]. It is hypothesized that the antibody titer of CST might be higher than that of other anti-m^{6}A antibodies. The regular concentration of CST (5 μg or even 2.5 μg) did not match well with low-input RNA (15 μg), possibly because a high antibody titer led to an excess of antibody binding to protein A/G. This resulted in crowded antibodies with numerous effective binding sites for m^{6}A, making it challenging for RNA containing m^{6}A to access and interact with the binding sites of antibodies. On the other hand, a lower concentration of CST (1.25 μg) created a suitable balance of antibody-bead complexes to effectively capture m^{6}A RNA fragments under optimized conditions. Furthermore, since M572 is a rabbit polyclonal antibody consisting of a heterogeneous mixture of antibodies targeting different epitopes, inconsistencies between batches may contribute to the diverse consensus motifs observed with M572[25]. In contrast, monoclonal antibodies such as M1006 and CST exhibited higher sensitivity and reproducibility than other polyclonal antibodies (Fig. 2G-I).

This study does have some limitations. We did not assess the lower limit of the CST antibody for 500 ng or even smaller amounts of RNA. Clinical samples often provide limited RNA, frequently less than 1 μg. Due to cost and time considerations, we did not use reduced concentrations of CST to conduct MeRIP-seq in a broader range of tissues. Nevertheless, given the current analysis, we are optimistic that CST at relatively low concentrations holds significant promise for effective performance in low-input RNA from various tissues across different species.

Conclusion

In this study, we conducted a comprehensive comparison of five commercially available anti-m^{6}A antibodies, offering a valuable guide for selecting antibodies in m^{6}A sequencing across diverse tissues and varying amounts of low-input RNA. Our findings revealed that standard concentrations of M572 and M1006 exhibited strong performance in the liver, whether from mice or humans, while CST demonstrated comparable results in the mouse brain. Additionally, reduced concentrations of CST demonstrated superior performance in m^{6}A sequencing from low-input RNA extracted from the human brain and liver. Looking ahead, future studies should explore CST's performance in a wider array of tissue types, particularly those with limited availability or low RNA yields, such as rare cell populations, human biopsies, or single-cell samples. Additionally, optimizing CST antibody concentrations for even lower RNA inputs, including sub-nanogram quantities, would enhance its utility for high-throughput even single-cell epitranscriptomic profiling.

Materials and methods

Tissues from adult mouse and human fetal donors, following human ethics and animal ethics guidelines

The human brain and liver were surgically removed from human first-trimester fetuses (9–13 weeks). Euthanasia for mice is performed using carbon dioxide (CO_2) inhalation followed by cervical dislocation. Mouse brains and livers were then collected from the same male C57BL/6 mice, aged 8 to 12 weeks. All methods were carried out in accordance with relevant guidelines and regulations. All experimental protocols involving humans and animals were approved by the Research Ethics Board of Suzhou Hospital affiliated with Nanjing Medical University, under ethics approval number 2019-002 Written informed consent was obtained from all subjects, or from a parent and/or legal guardian if subjects were under 16. All methods are reported in accordance with ARRIVE guidelines. The animal research procedures were implemented in accordance with the Animal Care and Use Committee of Nanjing Medical University. The human fetal samples were sourced from Suzhou Municipal Hospital, while the mouse samples were sourced from Nanjing Medical University. All sample collections were approved by an ethical review board, and the approval documents, along with the animal experiment licenses, are provided in the supplementary materials.

RNA isolation and DNase digestion

Total RNA was isolated from tissues using RNAiso plus (Takara, 9109) according to the manufacturer's instructions with jingxin technology multi-sample tissuelyser. Samples with high quality (28 S/18S > 2) were selected for further experiments. Since m^{6}A was also present in DNA, Turbo DNase (Invitrogen, AM2239) treatment was implemented to eliminate DNA contamination. A Qubit RNA HS Assay Kit (Thermo Fisher Scientific, Q32855) was employed to measure the RNA concentration.

MeRIP-seq of the brain and liver from human fetuses and mice

The procedure for MeRIP sequencing was slightly modified from the previously described low-input m^{6}A-seq protocol[18]. Briefly, 15 μg of total RNA was fragmented into 200-nt fragments with RNA Fragmentation Reagents (Thermo Fisher Scientific, AM8740). The fragmentation reaction was carried out in 70 °C for approximately 5 to 6 min in a preheated thermal cycler (Eastwin, ETC 821). Then, 2 μl of stop solution (0.5 M EDTA) was added to stop the reaction. The fragmented RNA was pelleted by ethanol precipitation. To prepare the m^{6}A input sample, 10 ng of the fragmented RNA was treated with the SMARTer Stranded Total RNA-Seq Kit v2-Pico Input Mammalian (Clontech, 634488) to construct a strand-specific RNA library. The remaining RNA was prepared for m^{6}A-seq: 30 μl protein G magnetic beads (Thermo Fisher Scientific, 10004D) and 30 μl protein A magnetic

beads (Thermo Fisher Scientific, 10002D) were mixed and washed twice with IP buffer (10 mM pH 7.5 Tris-HCl, 150 mM NaCl, and 0.1% IGEPAL CA-630), and then the mixed beads were resuspended in 200-μl IP buffer. Then, 5 μg anti-m^{6}A antibody (Darmstadt, Germany, Millipore, ABE572; Darmstadt, Germany, Millipore, MABE1006; Goettingen, Germany, Synaptic Systems, 202003; Danvers, Massachusetts, USA, Cell Signaling Technology, #56593; Waltham, Massachusetts, USA, Thermo Fisher Scientific, MA5-33030) was added to the resuspended beads, and the mixture was rotated at 4 °C overnight. After the combination of beads and antibody, the bead-antibody mixtures were washed twice with IP buffer and resuspended in 500-μl IP reaction buffer containing fragmented RNA and 5 μl Recombinant RNase Inhibitor (Takara, 2313B). After rotating at 4 °C for approximately 2 h, the bead-antibody-RNA mixtures were washed twice with IP buffer, washed twice with low-salt IP buffer (10 mM pH 7.5 Tris-HCl, 50 mM NaCl and 0.1% IGEPAL CA-630) and washed twice with high-salt IP buffer (10 mM pH 7.5 Tris-HCl, 500 mM NaCl and 0.1% IGEPAL CA-630). After the low/high salt wash, the bound RNA was eluted by competition with 6.7 mM N6-methyladenosine (Selleckchem, S3190). The 200-μl eluted RNA was mixed thoroughly with 1400 μl of 100% ethanol and 700 μl of RLT buffer. The mixture was loaded onto a RNeasy MiniElute spin column (Qiagen, 74104) and centrifuged at 12,000 rpm at 4 °C for 1 min. Then, the membrane of the spin column was washed with 500 μl RPE buffer once, then 500 μl 80% ethanol once, and finally centrifuged at 4 °C at full speed for 5 min. Then, 14 μl ultrapure H_2O was used to elute the m^{6}A RNA. The input RNA (10 ng fragmented RNA) and m^{6}A RNA were used as starting materials to construct libraries with SMARTer Stranded Total RNA-Seq Kit v2-Pico Input Mammalian (Takara-Clontech, 634488) according to the standard protocol. The input RNA was subjected to 14 PCR cycles, and the m^{6}A RNA was subjected to 16 cycles. The libraries were sequenced on an Illumina NovaSeq with a PE 150 bp read length.

m6A dot blot assay

Total RNA from each sample was diluted to the same concentration with ultrapure H_2O (Beyotime, ST876) and then denatured at 95 °C for 3 min. Then, 2 μl of total RNA was loaded onto NC membranes (Beyotime, FFN05) and UV crosslinked (1250 μJ UV, 48 s, 2 times). The membrane was washed with 1× PBST (10× PBS, Beyotime, ST448-1 L) for 3 min. Then, the membrane was washed with 5% nonfat milk at room temperature for 1 h and incubated with m^{6}A antibody (Millipore, MABE1006, 4 μg/μl) at 4 °C overnight. On the following day, the membrane was incubated with secondary antibody (Beyotime, A0216, A0208) at room temperature for 1 h. Then, the membrane was washed 4 times with 1× PBST for 10 min each. Finally, the m^{6}A signal was examined with a detection system (Tanon, GelCap All).

Reads pre-processing and alignment

First, Trim-Galore software was used to remove the splice and low-quality fragments of all the m^{6}A-seq and input raw data reads. Then, they were mapped with Bowtie2[26] (version 2.4.1) to the human reference genome (hg19) and reads mapped to rRNA were discarded. The remaining reads were mapped to human genome using HISAT2[27](version 2.2.1) with default parameters. Finally, the results obtained from HISAT2 were transformed into the bam format using BEDTools[28] (version 2.29.2).

Analysis of MeRIP-seq data

First, m^{6}A-enriched peaks from human tissues and mouse tissues were detected using MACS (2.2.7)[29] and input from human tissues and mouse tissues. Second, narrowPeak data obtained in MACS2 were annotated to the hg19 or mm10 reference genome from UCSC using the ChIPseeker (1.26.2) package[30]. We defined the m^{6}A methylation level of genes as the average value of the score value of corresponding m^{6}A peaks. Next, the package 'Guitar'[31] was used to analyze m^{6}A RNA-treated genomic features. All peaks were chosen for m^{6}A motif analysis with HOMER (v4.11)[32]. Then, annotation data were visualized by R software (version 4.0.3) and GraphPad Prism 8.

Peak intensity and the calculated overall m6A modification level

The methylation intensity of a corresponding region was calculated with (IPFPKM/InputFPKM), where Input FPKM is ((Counts of mapped fragments × 10^9) / (Length of peak × Total count of the mapped fragments)) and IPFPKM is ((Counts of mapped fragments × 10^9) / (Length of peak × Total count of the mapped m^{6}A fragments)) in MeRIP-seq. We identify the m^{6}A methylation level of the gene as $\frac{\Sigma_i^n \ m_i l_i}{L}$ $(i \in (1, 2, \ldots, n)$, where m_i is the methylation level, l_i is the length of the peak in the gene, n is the number of peaks located in the gene, and L is the longest transcript length of every gene). Enrichment of m^{6}A level was defined as the representation of the enrichment of the m^{6}A methylation level of all m^{6}A gene in each library.

Unique and overlapping tissue-specific m6A genes

The expression values calculated by the Genotype-Tissue Expression (GTEx) project and Tissue-specific Gene Expression and Regulation (TiGER) datasets were defined as tissue-specific genes. The file containing the median transcripts per million (TPM) of each gene was downloaded from version V8. The median TPM of each gene was ranked in decreasing order. Tissue-specific genes must meet two criteria: 1) the top 5 genes expressed in all tissues; and 2) > 90% of all genes expressed in particular tissues. Then, we merged these genes with the tissue-specific genes downloaded from the TiGER database to constitute a tissue-specific gene set[33]. Overlap between each kind of antibody library (M572, M1006, SY, CST and Ther) and the corresponding tissue-specific gene set (human brain, human liver, mouse brain and mouse liver). These overlapping genes were defined as overlapping tissue-specific m^{6}A genes. The remaining genes were defined as unique m^{6}A genes in each antibody library.

Motif discovery analysis

A de novo motif search was performed using HOMER (Version 4.11) in each antibody library. We selected the first "RRACH" motif from the obtained motifs of every antibody library (M572, M1006, SY, CST and Ther) and recorded the *p* value, using the '-mask -rna -len 8, 10, 12' parameters.

Statistical analysis

To assess antibody performance, we conducted statistical analyses using GraphPad Prism 8.0 software. Specifically, two-tailed Student's t tests were employed for comparisons. Results were considered statistically significant when the adjusted p value was less than 0.05. The significance thresholds were defined as follows: $^{*}p < 0.05$, $^{**}p < 0.01$, $^{***}p < 0.001$ and $^{****}p < 0.0001$. These analyses ensured robust comparisons across experimental conditions, facilitating an objective evaluation of antibody performance.

Data availability

The raw reads of the MeRIP-seq data were deposited into NCBI SRA under BioProject ID (PRJNA801897 and PRJNA801798) and accession number (SUB11014229 and SUB11001174) . The raw reads of the MeRIP-seq data were deposited into NCBI SRA under BioProject ID (PRJNA801897 and PRJNA801798) and accession number (SUB11014229 and SUB11001174) . The website link is https://www.ncbi.nlm.nih.gov/bioproject/PRJNA801897/ and https://www.ncbi.nlm.nih.gov/bioproject/?term=PRJNA801798.

Received: 9 May 2024; Accepted: 1 January 2025
Published online: 07 January 2025

References

1. Roundtree, I. A., Evans, M. E., Pan, T. & He, C. Dynamic RNA modifications in gene expression regulation. *Cell* **169**, 1187–1200. https://doi.org/10.1016/j.cell.2017.05.045 (2017).
2. Meyer, K. D. et al. Comprehensive analysis of mRNA methylation reveals enrichment in 3' UTRs and near stop codons. *Cell* **149**, 1635–1646. https://doi.org/10.1016/j.cell.2012.05.003 (2012).
3. Frye, M., Harada, B. T., Behm, M. & He, C. RNA modifications modulate gene expression during development. *Science* **361**, 1346–1349. https://doi.org/10.1126/science.aau1646 (2018).
4. Zhao, B. S. et al. M(6)A-dependent maternal mRNA clearance facilitates zebrafish maternal-to-zygotic transition. *Nature* **542**, 475–478. https://doi.org/10.1038/nature21355 (2017).
5. Cui, Q. et al. M(6)a RNA methylation regulates the self-renewal and tumorigenesis of glioblastoma stem cells. *Cell. Rep.* **18**, 2622–2634. https://doi.org/10.1016/j.celrep.2017.02.059 (2017).
6. Wang, X. et al. Structural basis of N(6)-adenosine methylation by the METTL3-METTL14 complex. *Nature* **542**, 260. https://doi.org/10.1038/nature21073 (2016).
7. Lin, Z. et al. Mettl3-/Mettl14-mediated mRNA N(6)-methyladenosine modulates murine spermatogenesis. *Cell. Res.* **27**, 1216–1230. https://doi.org/10.1038/cr.2017.117 (2017).
8. Sui, X. et al. METTL3-mediated m(6)A is required for murine oocyte maturation and maternal-to-zygotic transition. *Cell. Cycle* **19**, 391–404. https://doi.org/10.1080/15384101.2019.1711324 (2020).
9. Meng, T. G. et al. Mettl14 is required for mouse postimplantation development by facilitating epiblast maturation. *FASEB J.* **33**, 1179–1187. https://doi.org/10.1096/fj.201800719R (2019).
10. Wang, F. et al. N6-methyladenosine demethyltransferase FTO-mediated autophagy in malignant development of oral squamous cell carcinoma. *Oncogene* https://doi.org/10.1038/s41388-021-01820-7 (2021).
11. Zong, X. et al. The N6-methyladenosine RNA-binding protein YTHDF1 modulates the translation of TRAF6 to mediate the intestinal immune response. *Nucleic Acids Res.* https://doi.org/10.1093/nar/gkab343 (2021).
12. Chen, Z. et al. YTHDF2 is a potential target of AML1/ETO-HIF1alpha loop-mediated cell proliferation in t(8;21) AML. *Oncogene* https://doi.org/10.1038/s41388-021-01818-1 (2021).
13. Liu, J. et al. Landscape and regulation of m(6)A and m(6)Am methylome across human and mouse tissues. *Mol Cell* **77**, 426–440 e426 (2020). https://doi.org/10.1016/j.molcel.2019.09.032
14. Xiao, S. et al. The RNA N(6)-methyladenosine modification landscape of human fetal tissues. *Nat. Cell. Biol.* **21**, 651–661. https://doi.org/10.1038/s41556-019-0315-4 (2019).
15. Linder, B. et al. Single-nucleotide-resolution mapping of m6A and m6Am throughout the transcriptome. *Nat. Methods*. **12**, 767–772. https://doi.org/10.1038/nmeth.3453 (2015).
16. Garcia-Campos, M. A. et al. Deciphering the m(6)A code via antibody-independent quantitative profiling. *Cell* **178**, 731–747 e716 (2019). https://doi.org/10.1016/j.cell.2019.06.013
17. Meyer, K. D. DART-seq: An antibody-free method for global m(6)a detection. *Nat. Methods* **16**, 1275–1280. https://doi.org/10.1038/s41592-019-0570-0 (2019).
18. Zeng, Y. et al. Refined RIP-seq protocol for epitranscriptome analysis with low input materials. *PLoS Biol.* **16**, e2006092. https://doi.org/10.1371/journal.pbio.2006092 (2018).
19. Uhlen, M. et al. A proposal for validation of antibodies. *Nat. Methods* **13**, 823–827. https://doi.org/10.1038/nmeth.3995 (2016).
20. Wang, Y. F. In *Advanced Techniques in Diagnostic Microbiology: Volume 1: Techniques* (eds Tang, Y. W. & Stratton, C. W.) 127–147 (Springer, 2018).
21. Voskuil, J. Commercial antibodies and their validation. *F1000Res* **3**, 232. https://doi.org/10.12688/f1000research.4966.2 (2014).
22. Ke, S. et al. A majority of m6A residues are in the last exons, allowing the potential for 3' UTR regulation. *Genes Dev.* **29**, 2037–2053. https://doi.org/10.1101/gad.269415.115 (2015).
23. Busby, M. et al. Systematic comparison of monoclonal versus polyclonal antibodies for mapping histone modifications by ChIP-seq. *Epigenetics Chromatin*. **9**, 49. https://doi.org/10.1186/s13072-016-0100-6 (2016).
24. Timbury, M. C. *Notes on Medical Virology* (Churchill Livingstone, 1994).
25. Feederle, R. & Schepers, A. Antibodies specific for nucleic acid modifications. *RNA Biol.* **14**, 1089–1098. https://doi.org/10.1080/15476286.2017.1295905 (2017).
26. Langmead, B. & Salzberg, S. L. Fast gapped-read alignment with Bowtie 2. *Nat. Methods*. **9**, 357–359. https://doi.org/10.1038/nmeth.1923 (2012).
27. Kim, D., Langmead, B. & Salzberg, S. L. HISAT: A fast spliced aligner with low memory requirements. *Nat. Methods*. **12**, 357–360. https://doi.org/10.1038/nmeth.3317 (2015).
28. Quinlan, A. R. & Hall, I. M. BEDTools: A flexible suite of utilities for comparing genomic features. *Bioinformatics* **26**, 841–842. https://doi.org/10.1093/bioinformatics/btq033 (2010).

29. Zhang, Y. et al. Model-based analysis of ChIP-Seq (MACS). *Genome Biol.* **9**, R137. https://doi.org/10.1186/gb-2008-9-9-r137 (2008).
30. Yu, G., Wang, L. G. & He, Q. Y. ChIPseeker: An R/bioconductor package for chip peak annotation, comparison and visualization. *Bioinformatics* **31**, 2382–2383. https://doi.org/10.1093/bioinformatics/btv145 (2015).
31. Cui, X. et al. Guitar: An R/bioconductor package for gene annotation guided transcriptomic analysis of RNA-related genomic features. *Biomed. Res. Int.* 8367534 (2016). https://doi.org/10.1155/2016/8367534 (2016).
32. Zhou, Y. et al. Metascape provides a biologist-oriented resource for the analysis of systems-level datasets. *Nat. Commun.* **10**, 1523. https://doi.org/10.1038/s41467-019-09234-6 (2019).
33. Teng, S. et al. Tissue-specific transcription reprogramming promotes liver metastasis of colorectal cancer. *Cell. Res.* **30**, 34–49. https://doi.org/10.1038/s41422-019-0259-z (2020).

Acknowledgements
We thank the staff and students of the Suzhou Affiliated Hospital of Nanjing Medical University for their assistance.

Author contributions
Boxian Huang, Jiafeng Lu and Hong Li conceptualized and supervised the study, Liya Zhang and Wenjuan Xia performed most of the experiments and analyzed the data, Han Su and Jincheng Li performed the analysis for MeRIP-seq, Chunfeng Qian collected tissues and breed mice, Boxian Huang and Jiafeng Lu prepared the figures and wrote the paper.

Funding
This work was supported by the National Natural Science Foundation of China [grant numbers 82071720, 92168104, 81801478 ; Suzhou Talent Training Program [grant number GSWS2020057, GSWS2019005] ; Suzhou introduce expert team of clinical medicine [grant number SZYJTD201708] ; the Open Research Fund of State Key Laboratory of Bioelectronics, Southeast University [grant number SKLB2022-K02] ; and Suzhou key clinical diseases funding [grant number LCZX202109] .

Declarations

Competing interests
The authors declare no competing interests.

Ethics approval and consent to participate
The study was approved by the Medical Ethical Committee of Suzhou Municipal Hospital with the number of 2019-003 and all participants provided written informed consent.

Consent for publication
Not applicable.

Additional information
Supplementary Information The online version contains supplementary material available at https://doi.org/10.1038/s41598-025-85150-8.

Correspondence and requests for materials should be addressed to H.L. or B.H.

Reprints and permissions information is available at www.nature.com/reprints.

Publisher's note Springer Nature remains neutral with regard to jurisdictional claims in published maps and institutional affiliations.